Effect of constructing twin tunnels under a building supported by pile foundations in the Sydney central business district

Hadi Khabbaz, Robert Gibson, Behzad Fatahi *

School of Civil and Environmental Engineering, University of Technology Sydney (UTS), Australia

Abstract

In congested cities such as Sydney, competition for underground space escalates within the built environment because various assets require finite geotechnical strength and support. Specific problems such as damage to buildings may develop when high-rise buildings on piled foundations are subject to ground movements as tunnels are constructed. This paper focuses on the risks of tunneling beneath Sydney's Martin Place and how buildings are subject to additional loads caused by tunneling. The key objective of this study is to improve the understanding of tunnel–rock–pile interactions and to encourage sustainable development. A finite element model is developed to predict the interaction between tunnel construction and piled foundations. The tunnel, rock, and pile components are studied separately and are then combined into a single model. The ground model is based on the characteristics of Hawkesbury Sandstone and is developed through a desktop study. The piles are designed using Australian Standards and observations of high-rise buildings. The tunnel construction is modeled based on the construction sequence of a tunnel boring machine. After combining the components, a parametric study on the relationship between tunnel location, basements, and piles is conducted. Our findings, thus far, show that tunneling can increase the axial and flexural loads of piles, where the additional loading exceeds the structural capacity of some piles, especially those that are close to basement walls. The parametric study reveals a strong relationship between tunnel depth and lining stresses, while the relationship between tunnel depth and induced pile loads is less convincing. Furthermore, the horizontal tunnel position relative to piles shows a stronger relationship with pile loads. Further research into tunnel–rock–pile interactions is recommended, especially beneath basements, to substantiate the results of this study.
© 2019 Tongji University and Tongji University Press. Production and hosting by Elsevier B.V. on behalf of Owner. This is an open access article under the CC BY-NC-ND license (http://creativecommons.org/licenses/by-nc-nd/4.0/).

Keywords: Twin tunnels; Finite element modeling; Pile foundations; Plaxis; Sydney central business district

1 Introduction

Tunneling in Sydney is becoming more frequent because investment in underground transport infrastructure is an ongoing focus of public and private sectors. Within urban areas, it is important to consider the risks to people and assets at each phase of a project. Many techniques and strategies are adopted in the planning, design, and construction phases of a tunneling project to mitigate risks such as building damage and tunnel collapse. For example, planners impose restrictions on development, design engineers are required to follow careful judgment in their decision-making, and contractors must comply with community needs and quality requirements of the construction.

This study has been inspired by the Sydney Metro project, where twin tunnels of 6 m in diameter are to be constructed adjacent to and beneath a range of historical

---

* Corresponding author at: School of Civil and Environmental Engineering, Faculty of Engineering and Information Technology, University of Technology Sydney (UTS), City Campus, PO Box 123, Broadway, NSW 2007, Australia.

 E-mail addresses: Hadi.Khabbaz@uts.edu.au (H. Khabbaz), Robert.M.Gibson@alumni.uts.edu.au (R. Gibson), Behzad.Fatahi@uts.edu.au (B. Fatahi).

and modern structures within Sydney's central business district (CBD). This paper presents the response of existing buildings due to tunnel construction within shale and sandstone rocks. The commercially available software PLAXIS 2D (2015) has been used to model the tunnel–rock–pile interaction. Findings show that ground movements due to tunnel construction can increase the flexural and axial loads of existing building foundations, which may lead to building damage.

2 Background

Many studies (e.g., Franza et al., 2017; Mair, Taylor, & Burland, 1996; Potts & Addenbrooke, 1997) have approached the challenge of tunneling in adjacent buildings and piles using numerical, analytical, and empirical methods. A number of numerical studies (e.g., Nikolić, Roje-Bonacci, & Ibrahimbegović, 2016; Oliveira, 2014; Zhang, Liu, Huang, Kwok, & Teng, 2016) have focused on tunneling in soft soil, where stiff clay and granular materials are modeled using a typical Mohr–Coulomb model. There seems to be a lack of numerical studies and investigations into case histories about tunneling in jointed weathered rocks such as the Hawkesbury Sandstone formation, possibly because jointed weathered rocks exhibit unpredictable behavior, especially where rock joints are closely spaced within fault lines or dikes.

There are several analytical methods (e.g., Loganathan & Poulos, 1998; O'Reilly & New, 2015; Peck, 1969; Verruijt & Booker, 1996) that can be used for this analysis, but many assumptions are made regarding the performance of these calculations. It seems that the design should be modeled using a numerical analysis that can consider discontinuities in rocks or model the rock as an equivalent continuous material. Numerical analysis can also calculate reasonably complex interactions between tunnels and other structures. Therefore, engineers who design tunnels need to understand how to use advanced software packages so they can improve their predictions about ground behavior.

Empirical methods of analysis are dependent on rock classification systems, which are used throughout the design phases. The quality of rock will often govern how a tunnel should be designed, and the level of risk increases when the mechanical properties of the ground are difficult to test or predict. In contrast to tunneling in soft soils, the risks of tunneling in rock relate to the way that the rock is joined, the anisotropic behavior of the rock and the geology of the area. Rock mass classification systems are a practical tool that helps engineers, geologists, designers, and contractors to communicate the mechanical properties and predict rock mass behavior (Singh & Goel, 1999). Today, practicing engineers use a variety of methods to improve their understanding of rock mass material; the most common classification system being the rock mass rating introduced by Bieniawski (1989), the rock tunneling quality index initiated by Barton, Lien, and Lunde (1974),

and the geological strength index (GSI) developed by Marinos and Hoek (2000).

A major risk of a tunneling project is its interface with the urban environment. The risk is intensified by the method of excavation, geotechnical conditions, and location, e.g., if the tunnel is constructed in an urban area. Of particular interest is the potential for damage of historical masonry structures and modern, less rigid structures made from steel and concrete (Amorosi, Boldini, de Felice, Malena, & Sebastianelli, 2014). Such damage may include cracking, structural deformation, and a reduction in serviceability or a loss of structural integrity (Burland, 2012). The risk of such damages has been one of the factors that has led to the development of tunnel boring machines (TBMs), which aim to minimize the impact of tunneling activities on the surrounding environments.

Over the past few decades, numerous tunneling projects have been carried out in Sydney, such as the Northwest Rail Link and the Lane Cove tunnel. As a result, a large amount of data on the geotechnical conditions has been recorded. Bertuzzi (2014) improved previous work (Bertuzzi & Pells, 2002), and summarized the sandstone and shale parameters as a reference for other engineers. The values for sandstone and shale parameters are detailed in Tables 1 and 2, respectively.

The Hawkesbury Sandstone formation is classified as a weak rock that consists of fewer discontinuities than other rock masses such as shale. In the literature, two recent attempts to provide accurate geotechnical information of the Hawkesbury Sandstone and Ashfield Shale had been made by Bertuzzi (2014) and Oliveira (2014). Bertuzzi (2014) provided parameters for a continuum numerical analysis to find an equivalent rock mass by factoring the intact material properties based on the GSI and the Hoek–Brown failure criterion. Alternatively, the values provided by Oliveira (2014) may also be used for a discrete numerical study because they account for jointed rock behavior. Discrete models of jointed rock are useful when rock joints are likely to fail due to sliding or toppling rather than material failure such as spalling.

TBMs are often the preferred tunneling equipment in urban areas because of the relatively low construction noise and vibration. To minimize the impact on the urban environment, the construction sequence using the TBM is carefully designed to reduce volume loss, ground movements, noise, and vibrations (Cho, Kim, Won, & Kim, 2017). Moreover, more reduction in the noise and vibration aspects of the TBM have been achieved through the design improvement of cutting discs (Huo, Sun, Li, Li, & Sun, 2015).

An analysis of each step in the tunneling sequence yields a set of design requirements for lining a tunnel; therefore, when a segmental lining is analyzed, loads such as those caused by ground deformation, ground water pressure, and inherent forces of handling and stacking elements must be analyzed and considered so that tunnel lining strengthening techniques such as grouting can be implemented. A

Table 1
Characteristics of Hawkesbury Sandstone for tunneling purposes (Bertuzzi, 2014).

Parameter		Rock classification				
		I	II	III	IV	V
Uniaxial compressive strength, σ_{ci} (MPa)		30	25	15	10	5
Young's modulus, E_1 (MPa)		8 000	6 000	4 000	3 000	1 000
Unit weight, γ (kN/m³)		24	24	24	24	24
Poisson's ratio, v		0.25	0.25	0.25	0.25	0.3
Characteristic frictional constant, m_i		12	12	12	12	12
Mass Young's modulus, E_{mass} (MPa)		3 000	2 000	1 000	500	100
Geological strength index		75	65	55	45	35
Hoek–Brown	m_b	4.914	4.438	2.406	1.683	1.178
	s	0.062 2	0.020 5	0.006 7	0.002 2	0.000 7
	n	0.501	0.502	0.504	0.508	0.516
Mohr–Coulomb	c' (kPa)	1 000	500	300	200	150
	ϕ' (°)	55	50	50	40	35
	σ_t (kPa)	<300	<100	<40	<10	0

Table 2
Characteristics of Ashfield Shale for tunneling purposes (Bertuzzi, 2014).

Parameter		Rock classification				
		I	II	III	IV	V
Uniaxial compressive strength, σ_{ci} (MPa)		25	15	8	4	1
Young's modulus, E (MPa)		6 000	4 500	2 000	1 000	250
Unit weight, γ (kN/m³)		24	24	24	24	24
Poisson's ratio, v		0.25	0.25	0.25	0.25	0.3
Characteristic frictional constant, m_i		8	8	8	8	8
Mass Young's modulus, E_{mass} (MPa)		2 000	1 000	300	110	15
Geological strength index		55	50	40	30	20
Hoek–Brown	m_b	1.604	1.341	0.939	0.657	0.459
	s	0.006 7	0.003 9	0.001 3	0.000 4	0.000 1
	n	0.504	0.506	0.511	0.522	0.544
Mohr–Coulomb	c' (kPa)	400	250	150	90	40
	ϕ' (°)	45	40	35	25	15
	σ_t (kPa)	<100	<60	<10	0	0

tunnel designer may also manipulate the geometry of the lining rings to ensure that the forces transferred at the joints are considered.

When modeling the numeric behavior of the TBM construction, the sequences during tunnel excavation that cannot be represented by a two-dimensional case must be known. For example, Cho et al. (2017) stated that the hydraulic jacking forces that occur axially through a tunnel lining cannot be modeled using a two-dimensional analysis.

3 Methodology

3.1 Numerical studies

Tunneling adjacent to structures can cause additional risks to buildings and the built environment, and they may be difficult to detect. For instance, ground movements may cause joints to rotate, but they may not be large enough to affect reinforced concrete structures. However, if historic masonry structures are present, differential surface settlement may cause cracking in the walls due to tunneling activities close to the surface. Moreover, ground

movements may induce large forces into the piles, which might not have been considered in the original design.

In this study, several assumptions were made throughout the project, where engineering judgment was applied to simplify the model. These assumptions and limitations are as follows:

(1) The ground model did not consider the shale and alluvium deposits typically found in the first 2 m of borehole data from Sydney's CBD.
(2) The ground model in PLAXIS assumed that the values from Oliveira (2014) for ABAQUS software were sufficiently accurate to proceed with the jointed rock (JR) model in PLAXIS 2D.
(3) The building was assessed as an office building of 30 levels above the ground with 3 basement levels.
(4) Only static vertical loads were considered in the derivation of the building loads, and they included live and dead loads in accordance with AS 1170.
(5) The building simulation in PLAXIS was simplified to only model the piles and the axial loads to represent the main building response.

(6) The effect of ground water was not included in the analysis.

(7) To design the piles, an equivalent rectangular cross section was assumed based on an equivalent area and a calculation method to derive the equivalent centroid of reinforcement.

3.2 Sydney Metro City and Southwest tunneling project

An attempt was made to model the reduction in strength and serviceability of an existing building by emulating potential scenarios for constructing a tunnel adjacent to an existing building. Of special interest to this study is the proposed alignment of the Sydney Metro City and Southwest tunneling project because it passes beneath some of the tallest buildings in Martin Place, Sydney. Because historic sandstone buildings and modern tall, slender reinforced concrete structures are prominent in this area, of particular interest is the location where the tunnel passes approximately 23 m under a modern building on Bligh Street.

A desktop study was carried out to investigate the proposed tunnel alignment and the nature of typical ground materials supporting a multistory building in the CBD. Publicly available information such as geotechnical reports, Sydney Metro documentation, and published work on Hawkesbury Sandstone and Ashfield Shale material properties provided enough material data to apply judgment to model the research problem in PLAXIS 2D. Important boundary conditions and input parameters were also used in this desktop study.

A study of the tunnel alignment, as shown in Fig. 1, shows that the proposed 6 m diameter twin tunnels would pass from 23 m to 25 m beneath a modern building on Bligh Street (Metro, 2016). This 28-story building with four basement levels is a useful example when modeling the effects of tunneling adjacent to existing structures. This study based its assumptions on this case and also attempted to gather information from similar cases to build a realistic model.

The geology of the area below Martin Place has numerous features: Martin Place is underlain by fill and alluvium consisting of peaty quartz, silts, and clay (Ltd, 2012). Beneath the fill and soil, there are layers of Ashfield Shale and moderately weathered Hawkesbury Sandstone before reaching Class II or higher sandstone bedrock (Ltd, 2015). Hawkesbury Sandstone generally has high levels of in-situ horizontal stress, which increase with depth, and which is generally attributed to remnant tectonic stress and overburden pressure that leads to Poisson's effect (McQueen, 2004). The geological structure has two dominant features: the GPO Fault Zone and the Pittman LIV. The position of the dike is shown in relation to the approximate tunnel alignment in Fig. 2. These features are problematic in design and construction because it is very difficult to predict the sliding of rock wedges,

the ingress of water, or whether the tunnel would collapse.

The tunnel is likely to intersect the GPO Fault Zone at the intersection of O'Connell Street and Loftus Street, which creates further challenges to design and construction. The fault contains closely spaced and jointed/faulted weathered sandstone with a permeability of 100 L/(min m) or Lugeon (Ltd, 2012). This means that careful modeling, design, and construction are required to reduce the risk of rock spalling, shield instability, seepage forces, and tunnel collapse. The geology beneath Sydney's CBD is typically strong sandstone, which is usually considered to be predictable; however, geological features such as the Pittman LIV dike and GPO Fault Zone means that modeling the rock behavior for the design and construction of underground assets becomes uncertain. Not all of these geological features were modeled for this project due to the lack of published geotechnical information.

3.3 Preliminary ground model

A preliminary ground model was produced by synthesizing publicly available borehole information (Arup Pty Ltd, 2012; Bertuzzi, 2014; Coffey Geotechnics Pty Ltd, 2015; Oliveira, 2014). Table 3 indicates that the preliminary ground model is dominated by sandstone and shale, which are typical of Sydney's CBD.

According to borehole data, Class IV to III sandstone commences from 4 m to 6 m below ground level, north of the Pittman Dike at the intersection of Underwood and Pitt Street. Groundwater is present at approximately 0.5 m below the surface, where inflows are likely through the top permeable layers of fill and shale, while some inflows are also likely through the sandstone joints and bedding planes. From these assumptions of a ground model, further work can help develop the material parameters and construction sequences. By combining the information found in the borehole data and the material properties, the boundary conditions and input parameters were used for the PLAXIS 2D model.

3.4 Modeling a multistory building

After establishing the ground condition, a typical building was created to understand how the building loads would interact with the ground. These loads were calculated using a tributary area method down to the piles of this typical multistory building in the CBD. For this purpose, a 30-story building was selected, where the column spacing was set as 6 m and the height between levels as 3 m. The building shown in Fig. 3 has three 2.5 m high basement car parks, and the columns are 400 mm × 400 mm in the basement levels and 280 mm × 280 mm in the upper levels.

The result of calculating the loadings allows for a further analysis of the effect that structural design action has at the top of the piles for the proposed building. An anal-

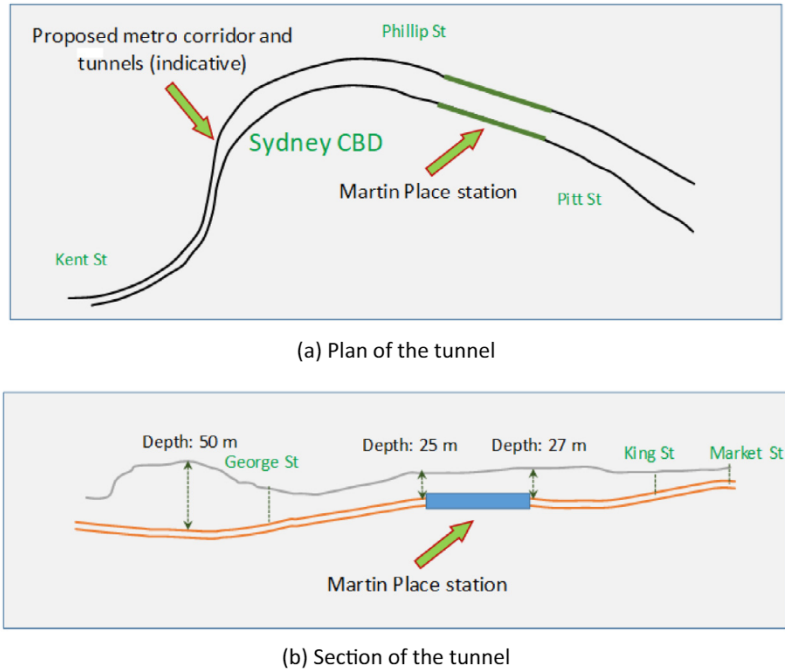(a) Plan of the tunnel

(b) Section of the tunnel

Fig. 1. Proposed tunnel alignment and station platform in Martin Place, (a) plan and (b) section (data taken from Metro, 2016).

Fig. 2. Geological features in Sydney's CBD (data taken form Pells, Braybrooke, & Och, 2004, and courtesy of Google for the background map).

Table 3
Preliminary ground model.

Geological formation	Class	Description	Depth
Fill and alluvium	N/A	–	0–0.5 m
Ashfield Shale	Class V or IV	Highly weathered sedimentary rock with low strength	0.5–2 m
Hawkesbury Sandstone	Class IV	Fractured sandstone, moderately to highly weathered	2–5.5 m
Hawkesbury Sandstone	Class III some Class II	Slightly fractured sandstone and siltstone, moderately weathered	5.5–16 m
Hawkesbury Sandstone	Class II or higher	Slightly weathered sandstone of high strength with little fractures	>16 m
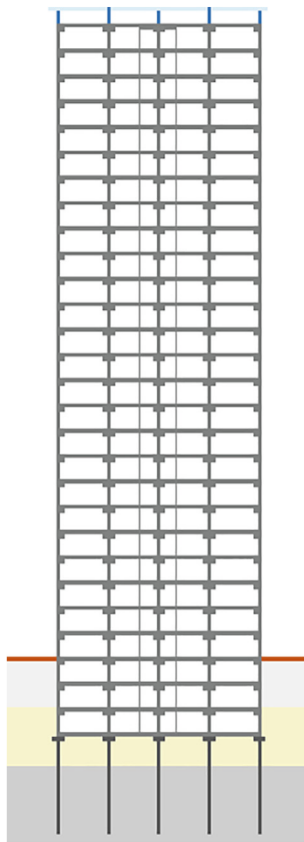
Fig. 3. Simplified building model including the pile foundations.

ysis in PLAXIS 2D enables the flexural forces that occur in the pile due to ground movements and second-order actions to be derived. The calculation of the loadings also allows for further analysis of the effect of structural design action at the top of the piles on the proposed building as presented in Table 4. An analysis in PLAXIS 2D enables the flexural forces that occur in the pile due to ground movements and second-order actions to be derived.

3.5 Foundation design of bored piles

Bored piles are commonly used when piling into sandstone in Sydney. The strength of the pile can be controlled by the structural strength of the hardened concrete pile or the geotechnical strength of the surrounding rock. The foundation load previously calculated is important when deciding on how to design a pile for this hypothetical

building model. Other parameters such as base resistance and skin resistance are documented in the paper by Pells, Mostyn, and Walker (1998). Further design equations and guidelines for strength and serviceability can be found in the Australian Standard for piling (Standards Australia, 2009a). Piles must be designed to meet the geotechnical strength and structural strength of the conditions in which they will be used. While the designer chooses the serviceability limits, they often depend on the type of structure that the foundations are holding. The geotechnical design of the pile presented in Table 5 uses the values of skin friction and base resistance for Class III sandstone, as adopted from the published work on foundation design by Pells et al. (1998).

The piling code AS2159–2009 (Standards Australia, 2009a) requires that the concrete code AS3600–2009 (Standards Australia, 2009b) be used to analyze the structural capacity of concrete piles. It also suggests that piles be treated similar to a column, but without buckling, unless used in very soft soils (Clause 5.2.3 AS2159–2009). With both columns and piles, the interaction diagram shows that the points from the ultimate squash load, balanced failure, unloading failure, and pure bending failure are used to determine structural adequacy. Table 6 depicts the properties of the reinforced concrete used to model piles. With a target of approximately 75%, the structural design capacity for piles is presented in Table 7.

After designing the piles for vertical forces, the horizontal forces are analyzed using PLAXIS 2D. Figure 4 shows the PLAXIS 2D output for a slice of the building shown in Fig. 3, where the blue and red areas represent the minimum deformation and maximum deformation, respectively. Piles 1 and 5 are edge piles, whereas piles 2, 3, and 4 are internal piles. Because a two-dimensional (2D) model has been selected, the forces in the out-of-plane direction and the corner piles have not been considered. To simulate the building, the piles were loaded for strength and serviceability such that the point forces act centrally to the pile, in accordance to Table 4. The resulting moment from this analysis was then used to design the piles for bending.

Piles 1 and 4 were further analyzed with interaction diagrams. However, to make the calculations less tedious, an equivalent square cross section with the same area as the circular pile was used and with the same natural axial distance from steel in compression and tension. Figures 5 and 6 show the calculations for the interaction diagrams. In both instances, the design is safe because the design

Table 4
Structural design action effect on top of piles.

Single column	Dead load (G)	Live load (Q)	Unfactored (G + Q)	Strength (1.35 G)	Strength ($N_d = E_d$) (1.2G + 1.5Q)	Long-term serviceability (G + 0.4Q)
Internal column (kN)	6 969	1 968	8 937	9 408	11 315	7 756
Edge column (kN)	3 587	898	4 486	4 843	5 652	3 947
Corner column (kN)	2 029	470	2 499	2 739	3 140	2 217

Table 5
Geotechnical strength for pile design.

Pile type	$\phi_{g,b}$	Pile diameter (mm)	Effective pile length* (m)	Effective A_s (m^2)	$f_{m,s}$ Class III (kPa)	A_b (m^2)	f_b (MPa)	Strength $R_{d,g}$ (kN)	Design capacity in strength
Internal piles	0.56	900	4	11.31	1 000	1.272	20	20 584	55%
Edge piles	0.56	600	4	7.54	1 000	0.565	20	10 556	54%
Corner piles	0.56	450	3	4.241	1 000	0.318	20	5 938	53%

* The first 1 m of the pile is assumed to have ineffective skin resistance.

Table 6
Reinforced concrete properties for piles.

Property	Value
Concrete compressive strength, f'_c (MPa)	40
Steel tensile yield, f_{sy} (MPa)	500
Young's Modulus concrete, E_c (GPa)	32.8
Young's Modulus steel, E_s (GPa)	200

Fig. 4. Analysis of design action effect for loaded piles.

bending and design axial forces are within the bounds of the allowable interaction. Therefore, the piling capacity was calculated by taking the distance from the origin to the point and then comparing it to the distance to the limiting values for the moment and normal forces while maintaining the gradient. Equation (1) was used to calculate the capacity ratio (CR) and limiting forces. The CR for the edge and internal piles was 97% and 84%, respectively.

$$CR = \frac{\sqrt{M_d^2 + N_d^2}}{\sqrt{M_{limit}^2 + N_{limit}^2}}, \qquad (1)$$

where M_d is design moment for pile design, M_{limit} is limiting moment along the interaction curve calculated as the intersection of the line with gradient N_d/M_d with the interaction curve, N_d is design axial force for pile design, and N_{limit} is limiting axial force along the interaction curve calculated as the intersection of the line with gradient N_d/M_d with the interaction curve.

The result of this analysis and design means that realistic values could be used in PLAXIS to measure the influence of adjacent tunneling on piled foundations. Piles were modeled in PLAXIS as rows of embedded beams; the parameters are summarized in Table 8. The multistory building was modeled in PLAXIS 2D after the design of the piles was finalized. Vertical loads acting on the piles were applied, while lateral loads such as wind were assumed to be negligible within the return period of tunnel construction. A 2D version of the model can be visualized by taking a slice of the building with a tributary width between column locations. The tributary for this slice of the building being modeled was 6 m, as listed in Table 8. The construction method produced reasonable stresses and displacements, such that the maximum vertical dis-
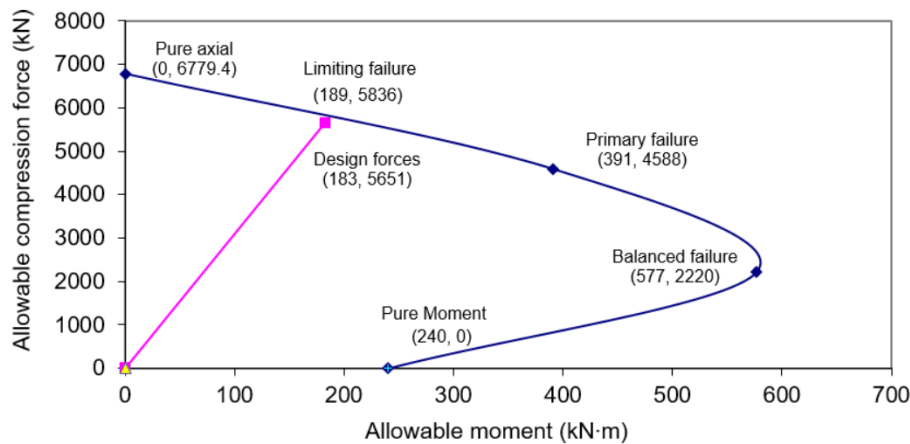
Table 7
Structural design for piles under axial loads.

Pile type	Pile diameter and number of vertical bars with 40 mm cover	Pile depth (m)	Axial capacity (kN)	Axial load for strength (kN)
Internal piles	$D_p = 900$ mm with 16N24 bars	5	15 733	11 315
Edge piles	$D_p = 600$ mm with 10N24 bars	5	7 124	5 652
Corner piles	$D_p = 450$ mm with 8N24 bars	5	4 256	3 140

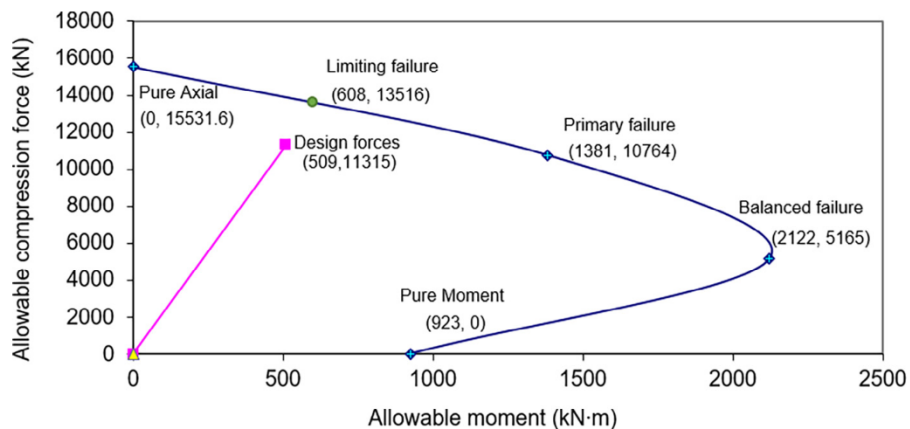Fig. 5. Edge pile 1 interaction diagram (designed in accordance with AS 2159 (2009a) and AS 3600 (2009b).

Fig. 6. Internal pile 4 interaction diagram (designed in accordance with AS 2159 (2009a) and AS 3600 (2009b).

Table 8
PLAXIS input parameters for piles.

Property	Edge Pile	Internal Pile	Comments
Young's modulus, E (kN/m^2)	3.539×10^7	3.539×10^7	Based on weighted average for the area of steel and concrete in the cross section
Unit weight, γ (kN/m^3)	25	25	–
Diameter, D_p (m)	0.6	0.9	–
Second moment of inertia, I (m^4)	6.362×10^{-3}	0.032	Assumed reinforcement increases I by a negligible amount
Out-of-plane spacing, $L_{spacing}$ (m)	6	6	–
Skin resistance start, $T_{skin,start}$ (kN/m)	1 478	2 800	Assumed skin resistance increases with depth
Skin resistance end, $T_{skin,end}$ (kN/m)	1 538	2 855	Assumed skin resistance increases with depth
Base resistance, f_b (kN)	6 362	11 310	–

placement in the pile due to the building load was approximately 2% of the pile diameter.

3.6 Ground material models

When using numerical software, it is important to ensure that the material models, boundary conditions, and input parameters are realistic and used correctly. To model the Hawkesbury Sandstone in PLAXIS 2D, only a bedding plane and a vertical plane were considered.

The Hoek–Brown (HB) model suggested by PLAXIS (2015) is a satisfactory method when modeling the behavior of rock, but the jointed rock (JR) model should be used if the rock joints and orientations are likely to cause failure. The key advantage of the HB method is the simplified calculation, whereby a jointed material is transformed into an effective and continuous homogenous material through the GSI classification. However, this method cannot model the anisotropic aspects of jointed rocks such as sandstone, whereas PLAXIS can consider jointed rock and anisotropy

through the JR model. Input parameters from Oliveira (2014) and Bertuzzi (2014) were validated using the HB and JR models in PLAXIS. A 6 m diameter twin tunnel was analyzed in a mass of layered rock 15 m below the surface, as shown in Fig. 7. While the boundary conditions remained constant, the output data were analyzed to compare the usefulness of each model with the sets of suggested parameters. A summary of all the material input data for sandstone is listed in Tables 9 and 10. These data have been used throughout the numerical study.
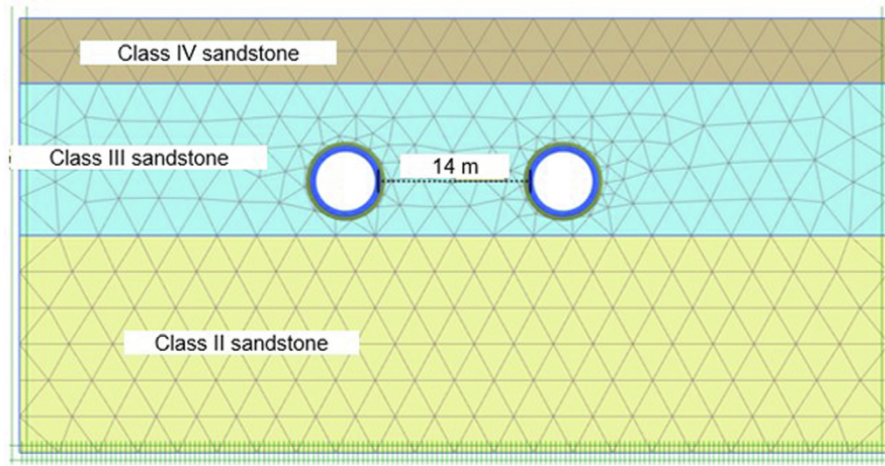
Fig. 7. Modelling a twin tunnel in layered Hawkesbury sandstone.

Table 9
Sandstone parameter values for Hoek–Brown PLAXIS material model.

Property	Class II Oliveira (2014)	Class II Bertuzzi (2014)	Class III Oliveira (2014)	Class III Bertuzzi (2014)	Class IV Oliveira (2014)	Class IV Bertuzzi (2014)
Unit weight, γ_{unsat} (kN/m^3)	24	24	23	24	23	24
Unit weight, γ_{sat} (kN/m^3)	24.5	24.5	23.5	24.5	23.5	24.5
Elastic modulus, E (MPa)	5 000	6 000	3 000	4 000	2 000	3 000
Poisson's ratio, v	0.2	0.25	0.25	0.25	0.25	0.25
Compressive strength, σ_{ci} (MPa)	25	25	12	15	5	10
Material constant, m_i	17	12	17	12	17	12
Geological strength index, GSI	70	65	60	55	50	45
Disturbance factor, D	0	0	0	0	0	0

Table 10
Sandstone parameter values for jointed rock PLAXIS material model.

Property	Class II Oliveira (2014)	Class II Bertuzzi (2014)	Class III Oliveira (2014)	Class III Bertuzzi (2014)	Class IV Oliveira (2014)	Class IV Bertuzzi (2014)
Unit weight, γ_{unsat} (kN/m^3)	24	24	23	24	23	24
Unit weight, γ_{sat} (kN/m^3)	24.5	24.5	23.5	24.5	23.5	24.5
Intact elastic modulus, E_1 (MPa)	5 000	6 000	3 000	4 000	2 000	3 000
Intact Poisson's ratio, v_1	0.2	0.25	0.25	0.25	0.25	0.25
Stratified elastic modulus, E_2 (MPa)	2 250	5 000	1 200	3 500	700	2 000
Stratified Poisson's ratio, v_2	0.2	0.25	0.25	0.25	0.25	0.25
Stratified shear modulus, G_2 (MPa)	250	600	160	400	110	100
Cohesion, c_{ref} (kPa)	5	50	5	35	5	15
Friction angle, σ (°)	35	30	32	25	32	20
Dilatancy angle, ψ (°)	12	12	7	7	5	5
Bedding angle, α_1 (°)	0	0	0	0	0	0
Tensile strength, σ_t (kPa)	5	50	5	35	5	15
Cohesion, c_{ref} (kPa)	5	50	5	35	5	15
Friction angle, ϕ (°)	35	30	32	25	32	20
Dilatancy angle, ψ (°)	12	12	7	7	5	5
Angle from horizontal, α_2 (°)	80	80	80	80	80	80
Tensile strength, σ_t (kPa)	5	50	5	35	5	15

The JR model produced better quality data and more realistic results for deformation and stress than the HB model. The greater variation shown in Fig. 8 demonstrates the reduced shear strength due to joints that were captured clearly by the JR model; similarly, the horizontal surface deformation for the JR model in Fig. 9 shows more variation.

This exercise showed the differences in the material models used by PLAXIS when calculating a tunnel excavation in virgin ground conditions. To predict the surface deformation, the JR model was better than Oliveira (2014) because it captured the rock joints and anisotropic behavior of the Hawkesbury Sandstone formation in detail.

3.7 Modeling the tunnel in PLAXIS

Twin tunnels that replicate the Sydney Metro tunneling project were modeled in PLAXIS 2D. The ground material parameters recommended by Oliveira (2014) were applied using the PLAXIS JR model. The construction sequence for the TBM can be modeled in two dimensions via a series of steps, which simulate the construction process. The 6 m diameter twin tunnels were modeled 20 m below the surface, where the tunnel lining had the properties listed in Table 11.

The twin tunnel model is represented through graphics of total deformation in Fig. 10. Here, the graphics show
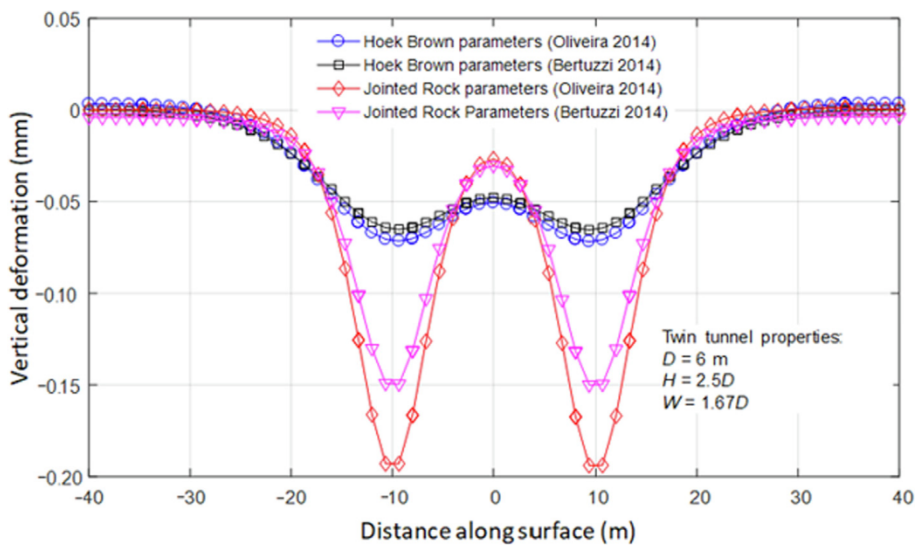

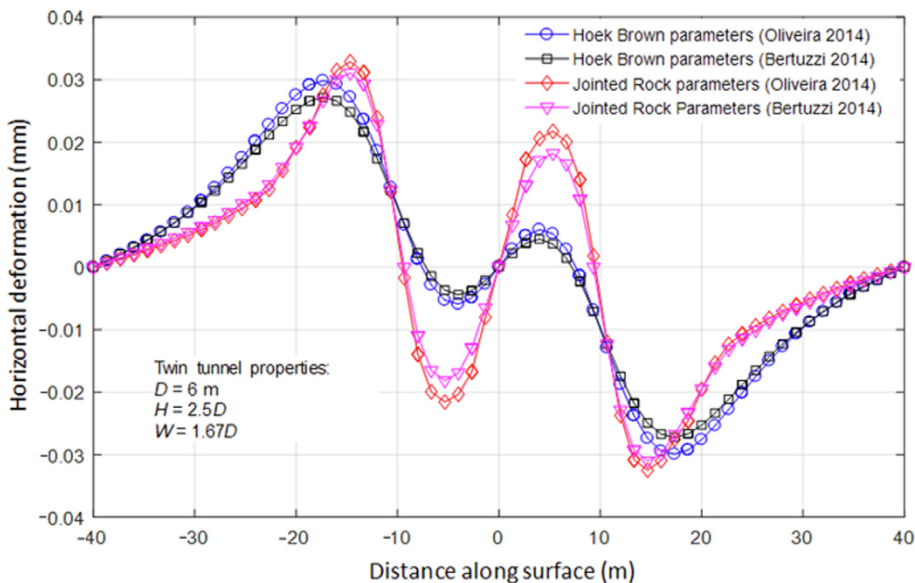Fig. 8. Vertical surface displacements calculated using PLAXIS material models.

Fig. 9. Horizontal surface displacements calculated using PLAXIS material models.

Table 11
Tunnel lining material properties.

Parameter	Value	Comments
Axial stiffness, EA (kN/m)	8.75×10^6	$\approx E_c \times t$
Flexural stiffness, EI (kN·m^2/m)	7.5×10^4	$\approx E_c \times \frac{t^3}{12}$
Lining thickness, t (m)	0.3	Assumed
Self-weight, w (kN/m/m)	7.5	$\approx 25 \, \text{kN/m}^3 \times t$
Poisson's ratio, υ	0.2	Assumed

the deformation and redistribution of stress caused by greenfield tunneling, where the ground has not been touched by pre-existing structures.

The information, parameters, material models, and PLAXIS 2D construction process techniques were combined to create the final tunnel–rock–pile interaction model. Figure 11 shows the model where Cluster 11, Cluster 12, and Cluster 4 represent Class IV sandstone, Class III sandstone, and Class II sandstone, respectively.

In the model it was assumed that the probability of the piles being fully loaded under the strength criterion at all times during construction was low. This assumption was based on the long-term serviceability of the building and the piles were loaded accordingly. The long-term serviceability load is described in Eq. (2) as

$$E_d = G + 0.4Q, \tag{2}$$

where G represents the dead load and Q denotes the live load.

The building loads at the top of the piles were taken from Table 4 as 7 756 kN and 3 947 kN for the internal and edge piles, respectively. While this assumption is less conservative, it is still valid because an office building is unlikely to be at full capacity at all times while the tunnel is being constructed.

The initial parameters were obtained from Bertuzzi (2014) and Oliveira (2014), and the ground was modeled in PLAXIS using the HB and JR material models. It was shown
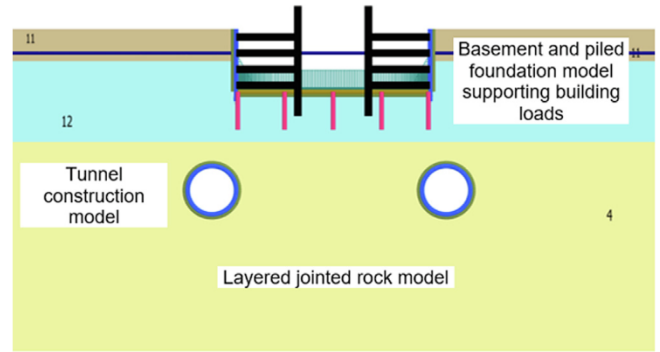

Fig. 11. Tunnel-rock-pile interaction model.

that the JR model delivered results capable of analyzing the anisotropic nature of jointed rocks such as Hawkesbury Sandstone. The components in this model included the ground and rock model, the excavation and construction sequence of the building, the excavation and construction sequence of the tunnels, and the final tunnel lining installation. The results are presented in the next section.

4 Results and discussion

This section presents the results and discussion of a numerical study of tunnel–rock–pile interactions. The results focus on how the pile and basement responded to tunneling, how the location of the tunnel and the building loads influenced the piles, and how the tunnel lining responded to the depth of alignment and distance from the loaded piles.

The findings show that tunneling adjacent to structures can affect the pile's flexural and axial loads and the tunnel location has a significant impact on the loads induced in the lining. However, the relationship between tunnel location and piles was less obvious even though the basement wall location had a significant impact on how the adjacent
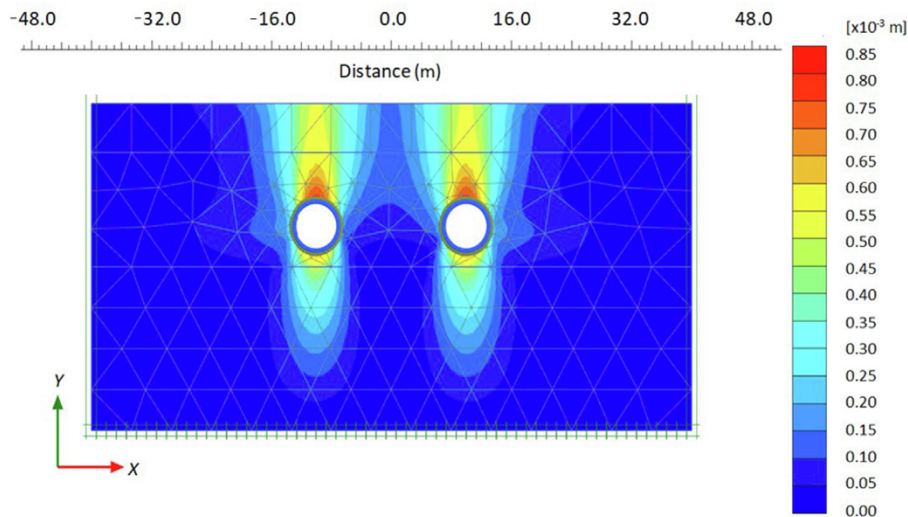

Fig. 10. Total deformations due to tunnel construction.

piles responded to nearby tunnel construction. Moreover, an increase in the building loads also increased how the pile responded before and after tunneling. Finally, an analysis of the tunnel lining shows how the hoop forces increased linearly with depth although the bending moments decreased at a much faster rate.

4.1 Response of piles to tunneling

The flexural loads on piles increased significantly during and after the tunneling phase, especially on those piles adjacent to the diaphragm wall. Table 12 shows the design CRs of Pile 1 before and after tunneling, as described by Eq. (1). This section will use the evidence to explain the results from the interaction model. The piles were designed by assuming that there would be no future tunnel and a CR of 97% with a phi factor of safety of 0.6 would suffice. This means that if a combination of flexural and axial loads on the piles were to increase, the pile would no longer meet the Australian Standards. If the allowance for safety factors also control other risks, the pile may still fail in compression or bending.

Table 13 and Fig. 12 show that the tunnel moved from a CR of 97% (Point *A*) to 123% (Point *B*), when the full load for the strength load case is applied, but when the serviceability load (Point *C*) is applied, the capacity of the pile increases to 102% and still does not meet AS 2159 and AS 3600. The chart has an interaction diagram, where the curved line shows all the points that cause structural failure in the pile. These points reveal the combinations of axial and compressive forces when the maximum load for strength and serviceability is applied. This result is troublesome for structural engineers, tunnel designers, and contractors because the person who designs the piles will not know how to account for future flexural loads induced into the pile after the tunnel has been constructed.

With internal Pile 2, Table 13 and Fig. 13 show a different feature, but in every instance, the ultimate moment does not exceed the minimum moment required by AS 2159. Furthermore, even if the bending moments induced by tunneling increased, the pile is still protected by the minimum flexural loads inherent in its original design. It appears that there is much less influence from tunnel construction on the change in flexural loading induced by tunneling.

Table 12
Reduction in edge Pile 1 structural capacity due to tunnel construction.

Aspect	Capacity ratio (%)	Result
Prior to tunneling (strength)	97	OK
After tunnel construction with ultimate axial load (strength)	123	Not good
After tunnel construction with serviceability load (serviceability)	102	Poor

Table 13
Reduction in internal Pile 2 structural capacity due to tunnel construction.

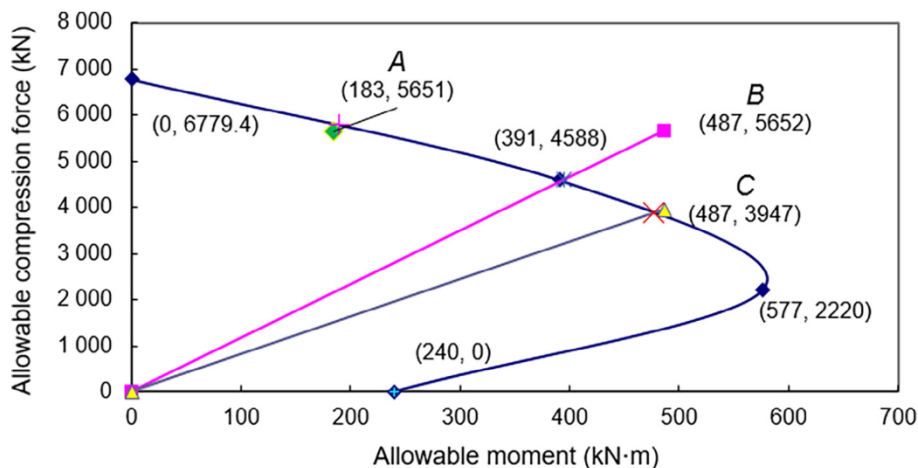| Aspect	Capacity Ratio (%)	Result
Prior to tunneling (strength)	84	Safe
After tunnel construction with ultimate axial load (strength)	84	Safe
After tunnel construction with serviceability load (serviceability)	61	Safe

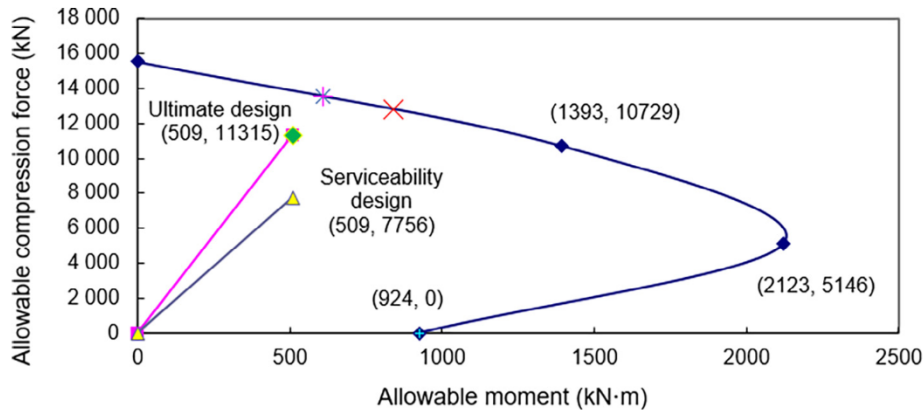Fig. 12. Structural capacity for edge pile 1 before and after tunneling.

Fig. 13. Structural capacity for internal pile 2 before and after tunneling.

The piling code, AS 2159, suggests that a designer should consider the potential for lateral ground movements, even though they are difficult to predict unless future events such as tunneling are known beforehand. This raises the question of where the responsibility lies when the structural features of a building may be compromised due to tunnel construction. The tunnel designers may argue that they are not at fault because the designers of the pile should have made an allowance for lateral ground movements. On the other hand, the pile designers would argue that they had no way of predicting such movements when the tunnel was being constructed. In reality, it would be unclear exactly what would happen if a pile founded on sandstone were to fail structurally because it could cause differential settlement as the pile moves further into the ground. The pile could also respond poorly to cyclic loading from wind and seismicity because the swaying of a tall building cannot transfer loads to the ground as the designers of the building intended. It is, therefore, recommended that further studies into how piles respond to tunneling should include cyclic loading on the pile and the effects of tunneling in jointed rock materials. Furthermore, because the interaction adjacent to basement walls is of interest owing to the extreme results of this study at these locations, alternative modeling techniques could also be used to compare the finite differences; this might also include discrete element and boundary element modeling.

4.2 Response of basements to tunneling

Before and after tunneling, the basement showed almost no impact due to ground settlement and induced bending moments, although excessive settlement may cause cracking in brittle finishes or excessive rotations in the concrete joints. While excessive bending moments in the basement slab may cause the slab to crack and fail, the settlement of the basement foundation is negligible. However, at the bottom of the basement walls, there was a settlement of approximately 4 mm. Figures 14 and 15 show the distribution of vertical displacement due to tunnel construction and the vertical displacement in the floor slab before and after construction, respectively. A negligible settlement of
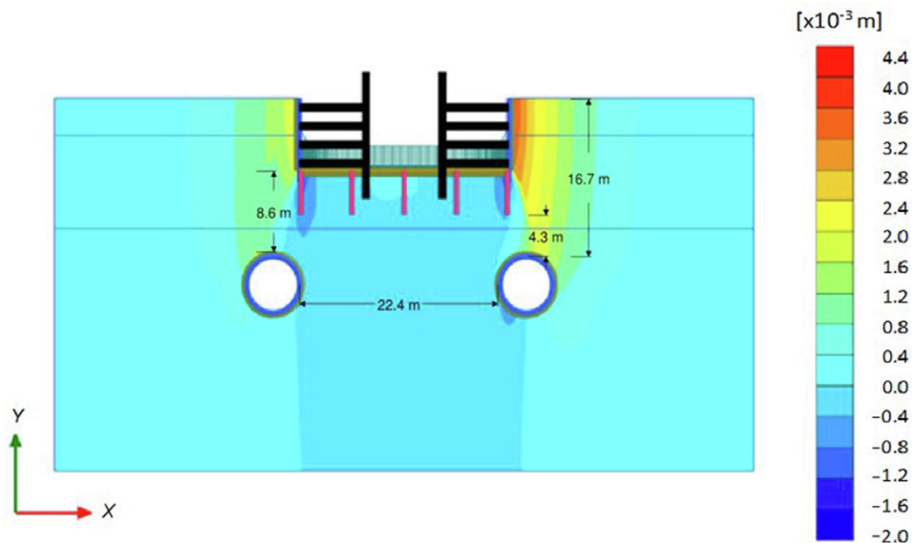

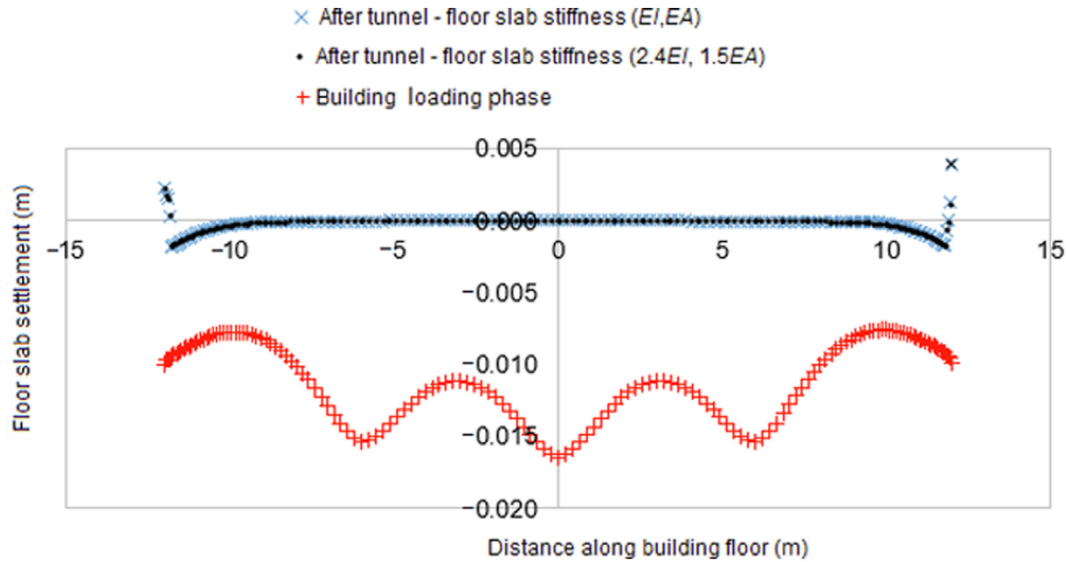Fig. 14. Location of tunnel installation.

Fig. 15. Floor slab settlement due to pile loading and tunnel construction (displacement reset to zero).

approximately 4 mm occurred adjacent to the basement walls; this settlement is insignificant because the concrete in the building is flexible enough to allow for such deformation.

The results of settlement were compared to the serviceability guidelines from Australian Standard AS 1170 (Standards Australia, 2002). When applying the long-term serviceability limit state described by Eq. (2), the midspan deflection for normal floor systems to control noticeable deflection is equal to the span length divided by 400. By taking the span length as the distance between columns, this limit becomes 6 000/400 = 15 mm. The deflections caused by the building loading phase on the piles are typically 5 mm between supports, which shows that the struc-

ture performed well in the serviceability limit state prior to tunnel construction. After the tunnel had been constructed, there was almost no settlement because the edge of the basement only deflected by approximately 4 mm. This deflection was consistent even after testing the stiffness of the slab. The floor became stiffer by a factor of 2.4 for flexural stiffness (EI) and by 1.5 for axial stiffness (EA), where the result showed that the influence due to changes in the ground slab deformation was insignificant.

However, if the building was a masonry structure, there could be some risks that the walls of this structure would crack. The midspan deflection limit for floors supporting existing masonry walls to control wall cracking is equal to the span length divided by 750 (Standards Australia,
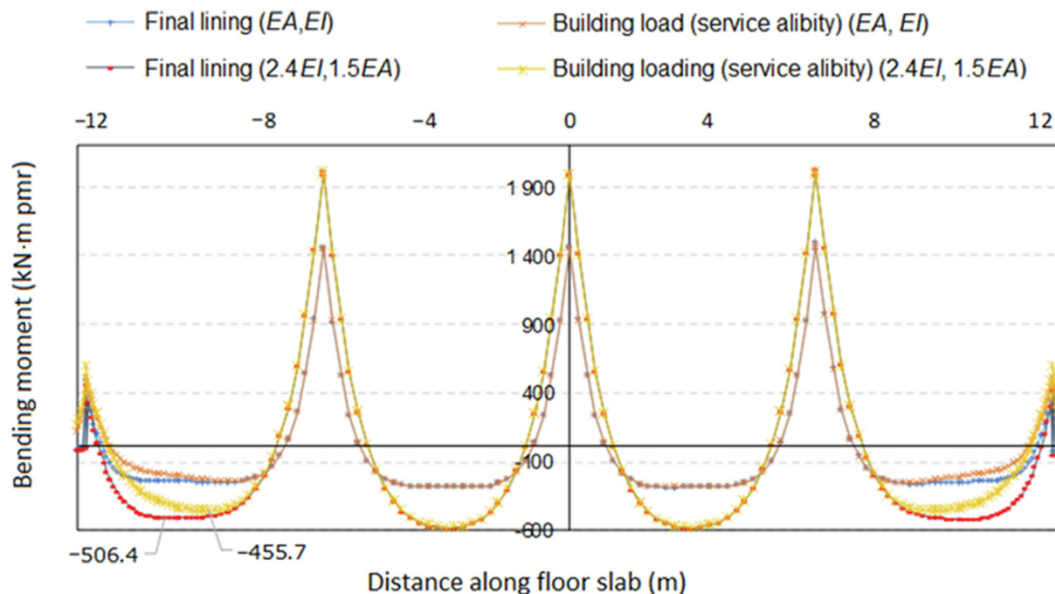

Fig. 16. Bending moments in the basement floor before and after tunnel construction.

AS 1170, 2002). Applying a limit of 6 000/750 = 8 mm shows that there is a moderate risk that the walls of masonry structures would experience minor cracking when subjected to tunneling at depths of 17 m below the surface.

The bending moments induced in the basement floor are also of interest when tunneling beneath basements because if the bending moments increase after tunneling, then the floor slabs could crack and they are costly to repair. Figure 16 shows the bending moments that occurred in the basement slab before and after tunneling; the stiffness of the slab was also increased so that this effect could be seen.

There was an insignificant change in the bending moments at almost every point before and after tunnel construction and between the different stiffness values analyzed, but the location adjacent to the basement walls induced greater bending moments into the slab; the maximum moment in this span increased by 12% from 455.7 kN m per meter run (pmr) to 504.5 kN m per meter run. To make matters worse, the maximum moment moved its location 1.3 m closer to the basement walls. This may not matter much if the slab was normally reinforced, but if the slab had been reinforced with post-tensioning, the change in location of the maximum moment could cause the slab to fail because post-tensioning applies magnitudes of compression in the inefficient regions of the slab.

5 Conclusions

This numerical study was carried out to determine the interactions between tunnel construction and piled foundations in jointed rocks with a special focus on tunneling within the CBD of Sydney. The response of a pile to tunneling was assessed successfully. This study makes a significant contribution to urban planning and the preliminary design of tunnels within urban environments because knowledge on the design aspects of piles and tunnel lining was used to assess the risks. Several key findings emerged from this study, namely the relationship between how a pile and a basement respond to tunneling, and the influence that piled foundations can have on tunnel linings. A specific result was observed at the junction of the basement walls and the edge pile. When examining the pile before and after construction, it was observed that in some instances, tunnel construction could significantly increase the flexural and axial loads that occur in a pile, particularly when the bending moments induced in an edge pile exceeded its original design capacity; the bending moments could cause a pile to fail due to nearby tunnel construction. The basement floor indicated negligible vertical deformation, but when assessing the increase in flexural loads, the results would be useful in practice. The bending moments in the space closest to the basement walls showed that the maximum moment shifted toward the walls and the magnitude increased slightly. If an existing slab was post-tensioned with steel, it could cause the post-tensioning to generate disruptive internal forces inside the slab. The result also pointed out that there is a relationship between a piled foundation and the internal forces of the lining. The hoop forces increased linearly with tunnel depth, while the bending moments decreased exponentially; this led to the creation of a design chart, which could also be developed for tunneling in the CBD of Sydney. This study may enhance sustainable development by encouraging urban planners to consider the relationship between existing buildings and future underground infrastructure.

If the increase in bending moments is coupled with other factors that draw on the built-in safety factors for the floor slab, such as poor construction, different geotechnical conditions, or incorrect design calculations, then cracking could possibly occur within this region due to the additional loads induced from tunneling. It is recommended that the regions adjacent to basement walls should be studied further to confirm the results of this study and to observe whether improved designs adjacent to basement walls can limit the forces that are induced by tunneling.

Declaration of Competing Interest

The authors certify that they have no conflict of interest or affiliations with any organization or entity with any financial interest in the subject matter or materials discussed in this manuscript. The authors have adopted publicly available information in relation to the Sydney Metro project in the formulation of the topic of interest. The assumptions made to develop the model only generally reflects the problem of tunneling beneath high rise structures. In reality, these types of interaction problems must be looked at in significantly more detail on a case by case basis to accurately inform planning, design and construction decisions.

References

Amorosi, A., Boldini, D., de Felice, G., Malena, M., & Sebastianelli, M. (2014). Tunnelling-induced deformation and damage on historical masonry structures. *Géotechnique, 64*(2), 118–130.
Arup Pty Ltd (2012). AMP Circular Quay Precinct, Multi-Disciplinary Engineering Services, Planning and Justification Report, Sydney.
Barton, N., Lien, R., & Lunde, J. (1974). Engineering classification of rock masses for the design of tunnel support. *Rock Mechanics, 6*(4), 189–236.
Bertuzzi, R. (2014). Sydney sandstone and shale parameters for tunnel design. *Australian Geomechanics, 49*(2), 1–10.
Bertuzzi, R., & Pells, P. J. N. (2002). Geotechnical parameters of Sydney sandstone and shale. *Australian Geomechanics, 37*(5), 41–54.
Bieniawski, Z. T. (1989). *Engineering rock mass classifications: a complete manual for engineers and geologists in mining, civil, and petroleum engineering.* New York: John Wiley & Sons.
Burland, J. B. (2012). *Chapter 26 Building response to ground movements.* ICE Manual for Geotechnical Engineering, Thomas Telford Ltd (pp. 281–296).
Cho, S. H., Kim, J., Won, J., & Kim, M. K. (2017). Effects of jack force and construction steps on the change of lining stresses in a TBM tunnel. *KSCE Journal of Civil Engineering, 21*(4), 1135–1146.

Coffey Geotechnics Pty Ltd (2015). Geotechnical Desk Study Report - 174-182 George Street and 33-35 Pitt Street, Sydney, Sydney.

Franza, A., Marshall, A. M., Haji, T., Abdelatif, A. O., Carbonari, S., & Morici, M. (2017). A simplified elastic analysis of tunnel-piled structure interaction. *Tunnelling and Underground Space Technology, 61*, 104–121.

Huo, J. Z., Sun, X. I., Li, G. Q., Li, T., & Sun, W. (2015). Multi-degree-of-freedom coupling dynamic characteristic of TBM disc cutter under shock excitation. *Journal of Central South University, 22*(9), 3326–3337.

Loganathan, N., & Poulos, H. G. (1998). Analytical prediction for tunnelling-induced ground movements in clays. *Journal of Geotechnical and Geo-environmental Engineering, 124*(9), 846–856.

Mair, R. J., Taylor, R. N., & Burland, J. B. (1996). Prediction of ground movements and assessments of risk of building damage due to bored tunnelling. In Paper presented to the International Conference of Geotechnical Aspects of Underground Construction in Soft Ground, Balkema, Rotterdam, viewed 11 May 2017 (pp. 713–718).

Marinos, P., & Hoek, E. (2000). GSI: A geologically friendly tool for rock mass strength estimation. In *GeoEng2000: An International Conference on Geotechnical & Geological Engineering* (pp. 1422–1442). Melbourne: International Society for Rock Mechanics.

McQueen, L. B. (2004). In situ rock stress and its effect in tunnels and deep excavations in Sydney. *Australian Geomechanics, 39*(3), 16.

Nikolić, M., Roje-Bonacci, T., & Ibrahimbegović, A. (2016). Overview of the numerical methods for the modelling of rock mechanics problems. *Pregled numeričkih metoda za modeliranje u mehanici stijena, 23*(2), 627–637.

O'Reilly, M. P., & New, B. M. (2015). Settlement above tunnels in the United Kingdom—their magnitude and prediction. *Tunnels & Tunnelling International, 20*(5), 56–66.

Oliveira, D. (2014). An alternative view on geotechnical parameters for tunnel design in Sydney. *Australian Geomechanics, 49*(3), 95–108.

Peck, R. B. (1969). Deep excavations and tunnelling in soft ground. In 7th International conference on soil mechanics and foundation engineering, State of the Art Volume (pp. 225–290).

Pells, P., Mostyn, G., & Walker, B. (1998). Foundations on sandstone and shale in the Sydney region. *Australian Geomechanics, 33*(3), 12.

Pells, P. J. N., Braybrooke, J. C., & Och, D. J. (2004). Map and selected details of near vertical structural features in the Sydney CBD. (2017-03-27). http://www.cityofsydney.nsw.gov.au/_data/assets/pdf_file/0010/143578/130617_PDC_ITEM05_ATTACHMENTA16.PDF.

Plaxis (2015). PLAXIS 2D - Input. Geotechnical Analysis Software, ver. 2015.02, PLAXIS, Delft, the Netherlands.

Potts, D., & Addenbrooke, T. (1997). A structure's influence on tunnelling induced ground movements. *Proceedings of the Institution of Civil Engineers-Geotechnical Engineering, 125*(2), 109–125.

Singh, B., & Goel, R. K. (1999). *Rock mass classification: a practical approach in civil engineering.* Elsevier.

Standards Australia (2002). AS1170 Structural design actions - General principles, Standards Australia, Sydney, Australia.

Standards Australia (2009). AS2159 Piling—Design and Installation, Standards Australia, Sydney, Australia.

Standards Australia (2009). AS3600 Concrete Structures, Standards Australia, Sydney, Australia.

Sydney Metro (2016). Environmental Impact Statement - Chatswood to Sydneyham, Sydney.

Verruijt, A., & Booker, J. R. (1996). Surface settlements due to deformation of a tunnel in an elastic half plane. *Géotechnique, 46*(4), 753–756.

Zhang, Z. X., Liu, C., Huang, X., Kwok, C. Y., & Teng, L. (2016). Three-dimensional finite-element analysis on ground responses during twin-tunnel construction using the URUP method. *Tunnelling and Underground Space Technology, 58*, 133–146.

Further Reading

Bateman, G. (2016). *Sydney Metro City & Southwest Technical Presentation.* Chatswood, Sydney: Seminar, Australiasian Tunnelling Society.

Guglielmetti, V., Grasso, P., Mahtab, A., & Xu, S. (2007). *Mechanized tunnelling in urban areas: Design methodology and construction control.* Routledge: Taylor & Francis.

Hoek, E., & Brown, E. T. (1997). Practical estimates of rock mass strength. *International Journal of Rock Mechanics and Mining Sciences, 34*(8), 1165–1186.

Infrastructure Australia (2016). Australian Infrastructure Plan - Priorities and reforms for our nation's future, Infrastructure Australia, Sydney.

Pells, P. (2011). Against limit state design in rock. *Tunnels & Tunnelling International*, 34–38.

Pells, P., & Bertuzzi, R. (2011). Limitations of rock mass classification systems for tunnel support designs. *Pells Sullivan Meynink Pty Ltd, vol,* 65.